Alexandria Engineering Journal 80 (2023) 383–396

Contents lists available at ScienceDirect

Alexandria Engineering Journal

journal homepage: www.elsevier.com/locate/aej

ORIGINAL ARTICLE

Quasi-Yagi antenna design for LTE applications and prediction of gain and directivity using machine learning approaches

Md. Ashraful Haque [a,b,*], M.A. Zakariya [a,c], Samir Salem Al-Bawri [d,e,**], Zubaida Yusoff [f,***], Mirajul Islam [g], Dipon Saha [a,b], Wazie M. Abdulkawi [h], Md Afzalur Rahman [b,d], Liton Chandra Paul [i]

[a] Department of Electrical and Electronic Engineering, Universiti Teknologi PETRONAS, Bandar Seri Iskandar 32610, Perak, Malaysia
[b] Department of Electrical and Electronic Engineering, Daffodil International University, Dhaka 1341, Bangladesh
[c] Smart Infrastructure Modelling and Monitoring (SIMM) Research Group Institute of Transportation and Infrastructure Universiti Teknologi PETRONAS, Bandar Seri Iskandar, 32610 Perak, Malaysia
[d] Space Science Centre, Climate Change Institute, Universiti Kebangsaan Malaysia (UKM), 43600, Bangi, Malaysia
[e] Department of Electronics & Communication Engineering, Faculty of Engineering & Petroleum, Hadhramout University, Al-Mukalla, 50512, Hadhramout, Yemen
[f] Faculty of Engineering, Multimedia University, Cyberjaya 63100, Selangor, Malaysia
[g] Dept. of Computer Science and Engineering, Daffodil International University, Dhaka 1341, Bangladesh
[h] Department of Electrical Engineering, College of Engineering in Wadi Addawasir, Prince Sattam bin Abdulaziz University, Al-Kharj 11991, Saudi Arabia
[i] Department of Electrical, Electronic and Communication Engineering, Pabna University of Science and Technology, Pabna, Bangladesh

ARTICLE INFO

Keywords:
Yagi antenna
Long-term evolution
CST
ADS
Machine learning

ABSTRACT

In recent years, improvements in wireless communication have led to the development of microstrip or patch antennas. The article discusses using simulation, measurement, an RLC equivalent circuit model, and machine learning to assess antenna performance. The antenna's dimensions are 1.01 $\lambda_0 \times 0.612\lambda_0$ with respect to the lowest operating frequency, the maximum achieved gain is 6.76 dB, the maximum directivity is 8.21 dBi, and the maximum efficiency is 83.05%. The prototype's measured return loss is compared to CST and ADS simulations. The prediction of gain and directivity of the antenna is determined using a different supervised regression machine learning (ML) method. The performance of ML models is measured by the variance score, R square, mean square error (MSE), mean absolute error (MAE), root mean square error (RMSE), and mean squared logarithmic error (MSLE), etc. With errors of less than unity and an accuracy of roughly 98%, Ridge regression gain prediction outperforms the other seven ML models. Gaussian process regression is the best method for predicting directivity. Finally, modeling results from CST and ADS, as well as measured and anticipated results from machine learning, reveal that the suggested antenna is a good candidate for LTE.

1. Introduction

Wireless cellular network technology has advanced significantly in recent years, paving the way for the creation of numerous new applications beyond basic phone conversations [1]. The data transfer rate, connection quality, and functionality of mobile devices have all improved with each new generation of technology [2]. Because of its high spectrum efficiency, high-speed transmission, and high data rate capabilities, the current mobile communication technology, known as Long Term Evolution (LTE), is being used in a significant number of mobile devices, including smartphones, laptops, and tablets [3]. LTE has an operational frequency that spans from 400 MHz all the way up to 4 GHz [4]. To fulfill the requirements of LTE applications Yagi-Uda antennas have been incorporated into a variety of unidirectional designs [5–7]. According to research [8,9], the end-fire gain and front-to-back ratio (FBR) of the Yagi antenna were both enhanced by applying the method

* Corresponding author at: Department of Electrical and Electronic Engineering, Universiti Teknologi PETRONAS, Bandar Seri Iskandar 32610, Perak, Malaysia.
** Corresponding author at: Space Science Centre, Climate Change Institute, Universiti Kebangsaan Malaysia (UKM), 43600, Bangi, Malaysia.
*** Corresponding author at: Faculty of Engineering, Multimedia University(MMU), 63100, Selangor, Malaysia.
E-mail addresses: md_21000832@utp.edu.my (M.A. Haque), samir@ukm.edu.my (S.S. Al-Bawri), zubaida@mmu.edu.my (Z. Yusoff).

https://doi.org/10.1016/j.aej.2023.08.059
Received 15 January 2023; Received in revised form 26 July 2023; Accepted 20 August 2023
Available online 1 September 2023

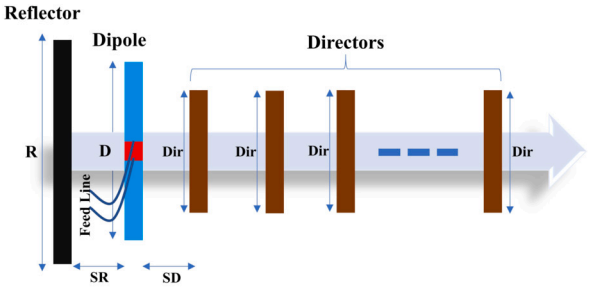

Fig. 1. Quasi-Yagi antenna structure.

of maximum power transmission efficiency (MMPTE). The design of the patch antenna can also be derived from a conventional dipole Yagi-Uda antenna, which is made up of two main elements: supply-driven and non-driven parasitic elements that consist of reflector and director elements, as shown in Fig. 1. A Yagi-Uda antenna is known for its high gain and narrower bandwidth, which can be controlled by manipulating its simple dipole array structure. Different design techniques of a Quasi-Yagi antenna have been presented with different performance levels and radiation characteristics [10,11]. In [12], a Quasi-Yagi antenna is proposed. Although the antenna has a very compact electrical size, the fractional bandwidth (FBW) is only 5.06%. A microstrip-fed millimeter-wave Yagi-Uda 1 × 2 array antenna is introduced in [13]. It provides a gain of 10 dB, but the size of the antenna is electrically large due to the array structure.

In this research work, a microstrip Quasi-Yagi antenna for 4G applications is proposed. The achieved gain is 6.32 dB, and the bandwidth is 0.377 GHz, while the size of the antenna is 130 × 119.30 mm^2. A comparison of numerous concurrently relevant works is shown in Table 1. Although the reflection coefficients in the cited works [14–20] are reported to be -18 dB, -31.55 dB, -35 dB, -25.02 dB, -32 dB, and -16 dB, respectively, in the suggested Yagi antenna, it is observed to be -50.44 dB in CST. In contrast to the 2.5 dBi, 6.0 dBi, 4.27 dBi, 5.02 dBi, 5 dBi, 2.5 dBi, and 2.0 dBi indicated in the comparison table, the proposed design has a peak gain of 6.76 dBi. The radiation efficiencies of the reference works [15,16] and [18,19] are 73%, 80%, and 96%, 66% respectively; however, the efficiency of the proposed Quasi-Yagi antenna is 83.05%. Even though machine learning-based investigations are not used in the aforementioned references in the table, they are heavily utilized in the design that has been provided. The optimization process can be sped up with the help of regression methods because their ML evaluation is considerably faster than the numerical solution of a physical simulation model such as CST, HFSS, and ADS. Regression models also help isolate the role of each design element in producing the desired results. The results of the simulation and the predictions are identical to one another. Additionally, our work includes the analysis of the equivalent RLC circuit of the proposed design, which is not included in the previously cited literature. Finally, we obtained extremely good agreement between the findings of the designed equivalent circuit and those obtained through simulation and measurement. Our proposed Yagi antenna is economical due to the use of low-cost material and possesses excellent performance in the intended operational LTE band. This paper is unique in that it combines the integration of simulation, measurement, and construction of the RLC equivalent circuit model with a comparison of the CST result with Agilent ADS, as well as the use of multiple regression models to evaluate the performance and errors of the proposed antenna.

The antenna is modeled in a 3D electromagnetic simulation environment using a tool such as CST, HFSS, FEKO, ADS, and so on, each of which uses a slightly different computational method. Researchers have found that using machine learning (ML) techniques to optimize antenna design, predict results, and choose antennas for wireless applications [21–27], which helps to alleviate some of the restrictions. Modeling an antenna with ML can boost its performance and precision. The predictive model is obtained in the form of a data set by training ML models to actualize the linkage between input and output parameters. Through trial and error, the training process determines which model parameters will yield the most accurate predictions for the data being analyzed [28]. Antenna modeling with CST Microwave Studio yields a data set including return loss, resonant frequency, reflector, director, and driving element length of the Yagi antenna. The resonance frequency used in the simulation is between 1 and 3 GHz [29]. To achieve the desired dimensions and resonance frequencies, the authors of [30] proposed using an ANN to design a microstrip patch antenna. However, error percentages such as MSE, MAE, MSLE, and MAPE were not considered. The proposed ANN model's prediction outcomes were not validated against other ML models. The resonant frequency of a patch antenna is predicted by artificial neural networks in [31,32]. In this research, the error percentage was computed by dividing the actual value by the anticipated value. Notably, the percentage of error in terms of MSE, MAE, MSLE, MAPE, and RMSLE was not analyzed in the state-of-the-art studies conducted recently. Furthermore, most of the existing publications on ML-based antenna design do not assess the accuracy in terms of variance score or R squared. Different methods, including linear regression, random forest regression, decision tree regression, lasso regression, ridge regression, extreme gradient boosting regression, bayesian linear regression, and ridge regression, are then used to make predictions. To examine the performance of proposed regression analysis approaches, simulation, measurement, and computed resonant frequency values were compared with performance metrics. Mean absolute error (MAE), median error (ME), mean squared error (MSE), mean absolute percentage error (MAPE), and mean squared logarithmic error (MSLE).

The antenna performance is designed and optimized with the help of CST MWS simulation software. Furthermore, the same antenna is fabricated for measurement and verified with the simulation result. Return loss and bandwidth are verified using the Advance Design System (ADS) circuit simulation tool by employing the R-L-C equivalent circuit. Multiple supervised regression algorithms implemented in the electromagnetic (EM) simulation tool CST have recently been investigated as a means of predicting the directivity and gain. In order to verify this, a survey of Quasi-Yagi antennas developed specifically for LTE applications is shown in Table 1, and this survey is compared to the suggested design.

2. Research gap and contribution

As highlighted earlier, the Quasi-Yagi antenna majority of available designs incorporate machine learning. Our proposed, designed antenna can perform to the capabilities in terms of gain, return loss, and efficiency. This article combines various regression models to simulate, measure, and build the RLC equivalent circuit model.

The main contribution of this study is summarized as follows:

- Regression methods are useful for optimizing processes since their ML assessment is much quicker than the numerical solution of a physical simulation model.
- Regression models also help isolate the role of each design element in producing the desired results. The results of the simulation and the predictions are identical to one another.
- The results of the constructed RLC equivalent circuit were found to be in excellent agreement with those obtained from simulation and experiment.

3. Antenna design and configuration

The CST (Computer Simulation Technology) tool is used to develop and simulate the dual-band Quasi-Yagi antenna. Antenna components

Table 1
Performance comparisons with the published state of the art.

Parameters	Ref. [14]	Ref. [15]	Ref. [16]	Ref. [17]	Ref. [18]	Ref. [19]	Ref. [20]	Proposed
Technique	Reconfigurable	Quasi-Yagi antenna	Dielectric resonator antenna	Slotted array antenna	Finite integration technique	Planar antenna	Planar antenna	Quasi-Yagi antenna
Application	LTE	LTE	5G Communi-cation	28 GHz 5G mobile	WLAN, WiMAX	LTE, GSM, UMTS	WLAN, LTE	LTE
Return Loss (dB)	-18	-65.23, -31.55	-35	-25.02	-32	-32	-16	-50.44
Bandwidth (GHz)	1.85 - 2.6	1.65 - 1.95 2.5 - 2.72	3.3 - 4.2	27.03 - 28.82	2.2 - 8	1.37 - 4	1.98 - 2.1 2.71 - 2.82	1.78 - 1.95 2.52 - 2.85
Max Gain (dBi)	2.5	6	4.27	5.02	5	2.5	2	6.76
Efficiency %	—	73	80	—	96	66	—	83.05
ML Investigation	No	No	No	No	No	No	No	Yes
RLC Equivalent Circuit Analysis	Yes	No	No	No	No	No	No	Yes
Size (W×L) (mm^2)	0.30 λ_0× 0.152 λ_0	1.08 λ_0× 0.59λ_0	0.29 λ_0× 0.19 λ_0	13.63 λ_0× 6.36 λ_0	0.7 λ_0× 0.467 λ_0	0.089 λ_0× 0.203 λ_0	0.192 λ_0× 0.192 λ_0	1.01 λ_0× 0.612 λ_0
Substrate Material	FR4	FR-4	FR-4	Arlon/ AD430	FR-4	FR-4	FR-4	FR-4

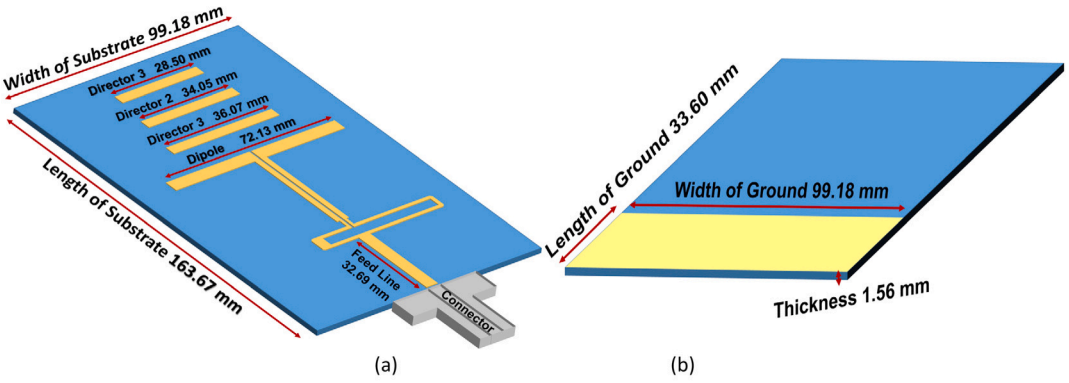

(a)The Geometry of Quasi-Yagi Antenna. (Front) (b) Quasi-Yagi Antenna. (Back)

Fig. 2. (a)The Geometry of Quasi-Yagi Antenna. (Front) (b) Quasi-Yagi Antenna. (Back).

include a driving element, three director elements, and copper metal, which is used as the ground plane in this implementation. As substrate properties, FR-4 features a dielectric constant of 4.3 and a loss tangent of 0.025, while the thicknesses of the copper metal and the substrate are 0.035 mm and 1.56 mm, respectively. A Microstrip (MS) to Co-planar Strip Line (CPS) feeding technique is used for impedance matching, where a balun phase shifter and a quarter-wave transformer are constructed at the input port of the antenna. In order to match the power lines between the microstrip line and the balun phase shifter for this feeding technique, the quarter-wave transformer line with a characteristic impedance of Z_1 is used [33].

$$Z_1 = \sqrt{\frac{Z_0}{Z_L}} \tag{1}$$

Where, Z_0 = inductance per unit length of line, and Z_L = capacitance per unit length of line.

The balun phase shifter is used to balance the feeding for the CPS at both operating frequencies of 1.85 GHz and 2.64 GHz by generating a 180° phase difference between the MS and the CPS [34]. The parameters of the antenna, such as the length of the driven element, number of director elements, and dielectric thickness, are studied to design the antenna to operate at the proposed frequency band. The geometry configurations of the proposed antenna are shown in Fig. 2 (a), and the back view is introduced in Fig. 2 (b).

4. Working principle

The simulated current distribution is analyzed and explained to provide light on the attributes and operating principles of the proposed antenna.

4.1. Current distribution

The distribution of the current at a number of different frequencies is shown in Fig. 3. At 1.85 GHz, the highest surface current is 42.6429 A/m, while at 2.64 GHz, the peak surface current is 41.4156 A/m. The production of the first operational band can be traced back to the increased current density that can be found in the feed line's lowermost segment. The production of the second working band of the Yagi antenna is attributable to the increased current density that may be found at the top part of the feed line of the directors.

5. Parametric study

The subsequent sections show the effect of the structure's primary characteristics to help readers better grasp its workings.

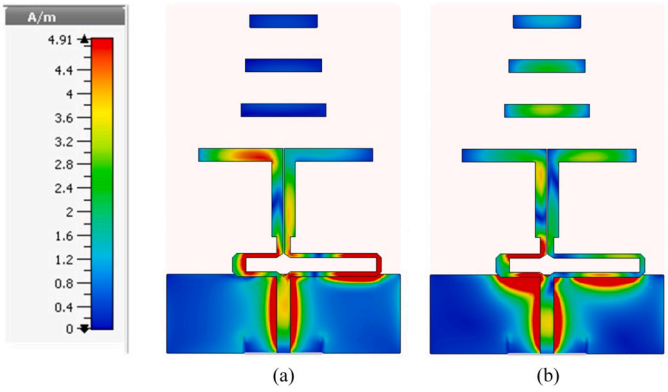

Fig. 3. Simulated current distribution of the proposed antenna at (a) 1.85 GHz and (b) 2.64 GHz.

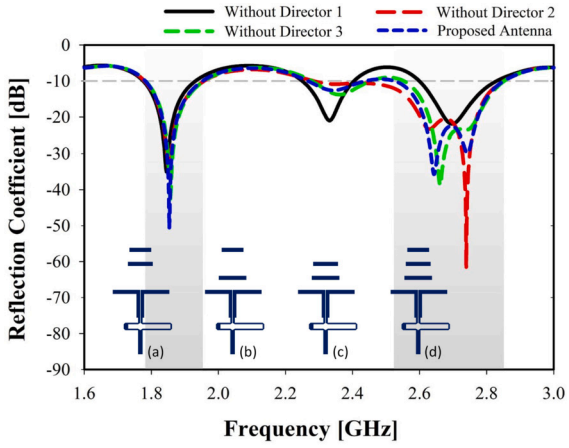

Fig. 4. Simulated reflection coefficient for different directors (a) Without director 1 (b) Without director 2 (c) Without director 3 (d) With all directors (proposed antenna).

5.1. Director of Yagi antenna

Due to its capacitive nature, the element on the right side of the Yagi antenna called the director, is responsible for focusing the radiated power along the director components [35]. The multiband operation of the proposed antenna is displayed in Fig. 4, both in the absence and presence of directors. When using three directors at once, the antenna clearly displays the optimal S11 curve. Moreover, the gain of the antenna is proportional to the number of directors placed after the dipole [36]. Fig. 5 shows the proposed antenna operating in dual bands, both without and with directors. Gains of about 5 dB are possible when Director 1 is removed, while gains of around 6 dB are possible when Directors 2 and 3 are removed. The maximum gain is about 7 dB when all three directors are considered.

5.2. Balun microstrip feed

A microstrip line (MS) or other unbalanced transmission line is converted into a balanced coplanar stripline through a balun (CPS). Many scientists are interested in developing a realistic, high-performance MS-to-CPS balun (or transition) [37]. A good dominance of the reflection coefficient of the Quasi-Yagi antenna is seen when the length of the balun microstrip feed line, represented by (Lb), is increased from 36 to 41 mm, as shown in Fig. 6. The S11 value does not extend to the resonant frequencies needed for the LTE applications requested for Lb = 36 mm, 38 mm, and 41 mm. For Lb = 39.5 mm, the antenna provides the expected coverage.

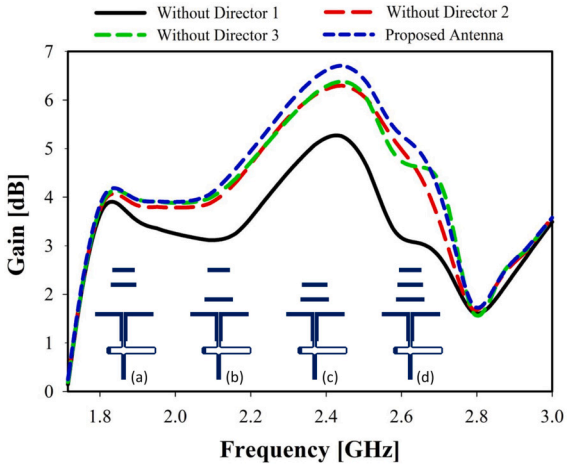

Fig. 5. Simulated gain for different directors (a) Without director 1 (b) Without director 2 (c) Without director 3 (d) With all directors (proposed antenna).

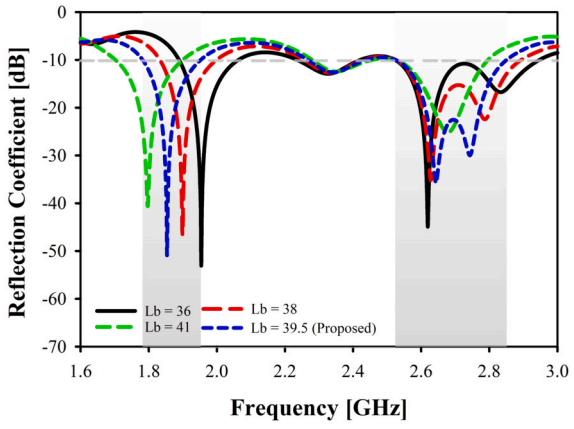

Fig. 6. Simulation of the reflection coefficient for several lengths of microstrip baluns.

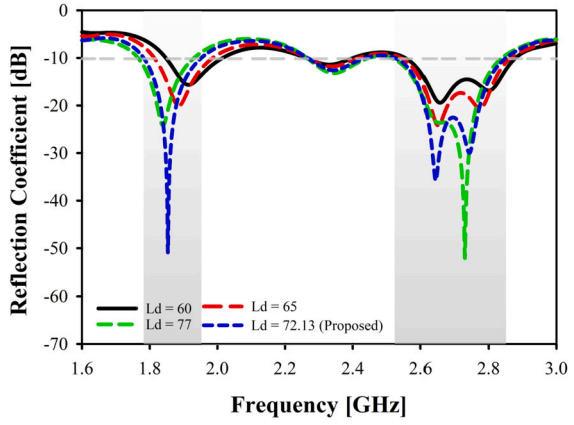

Fig. 7. Simulation of the reflection coefficient for different dipoles of the Quasi-Yagi antenna.

5.3. Driven element of Yagi antenna

Because it links the Yagi antenna to its power supply and acts as the feed via which the antenna is activated, the driver element is often regarded as the most crucial part of the antenna. The Yagi antenna's input impedance and primary resonance frequency are both within the control of the antenna's geometry [15]. It has been discovered that the return loss increases with the driven element's length. The proposed

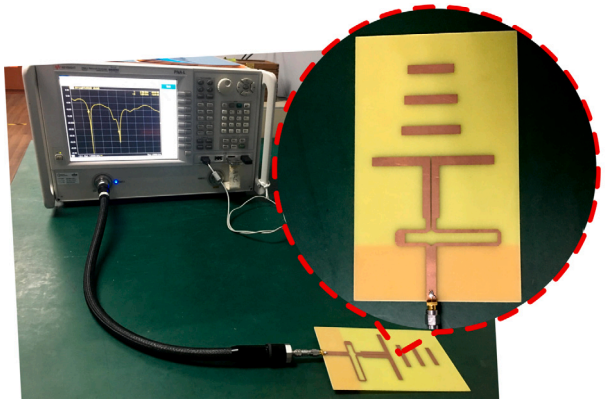

(a) S11 measurement using VNA

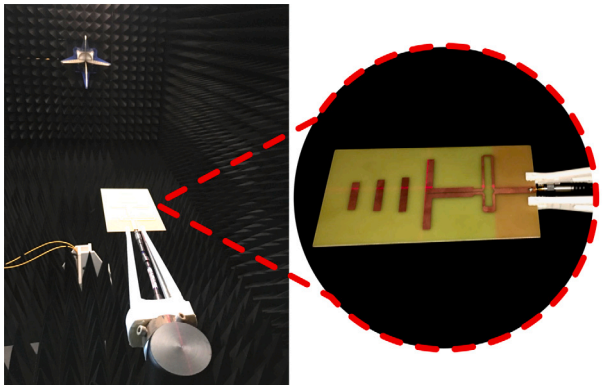

(b) Radiation characteristics measurement within anechoic chamber

Fig. 8. Measurement setup.

value of return loss is significantly lower than the actual value for the length of the driven element (Ld) = 60 mm and 65 mm. For Ld = 77, the return loss is extremely large, but the second desirable resonance frequency is not obtained, as depicted in Fig. 7. However, the recommended Ld = 72.13 has been found to be superior to alternative solutions in terms of desired resonant frequencies, such as 1.85 and 2.64 GHz.

6. Result analysis

This section discusses the proposed MPA's simulated and measured results. Additionally, the simulated S^{11} utilizing CST is compared to the measured result and the equivalent circuit model from Advanced Design System (ADS). Finally, alternative machine-learning learning approaches for predicting the proposed antenna's resonance frequency are briefly examined. Return loss (S11) indicates the amount of power reflected in a transmission line. An antenna must have a minimum of -10 dB in order to function efficiently [38].

A vector network analyzer (VNA) is used to test the port properties, as shown in Fig. 8, while an anechoic chamber is used to assess the radiation properties. Fig. 9 depicts a simulated return loss graph for the optimized antenna, with two resonance frequencies offered by the Yagi antenna: 1.85 GHz and 2.64 GHz, with corresponding return loss magnitudes of S_{11} of -50.44 dB and -35.67 dB, respectively. A vector network analyzer (VNA) can be used to measure an antenna's S_{11}. The measured return loss of the fabricated antenna is shown in Fig. 9. Resonance at 1.88 GHz and 2.62 GHz has been reported to be as low as -37.90 decibels (dB) and as high as -22.74 decibels (dB). The resonance shifts from 1.85 GHz to 1.80 GHz and from 2.64 GHz to 2.76 GHz when the simulation and the experimental results are compared. In the simulation, the antenna is energized using a waveguide port; in practice,

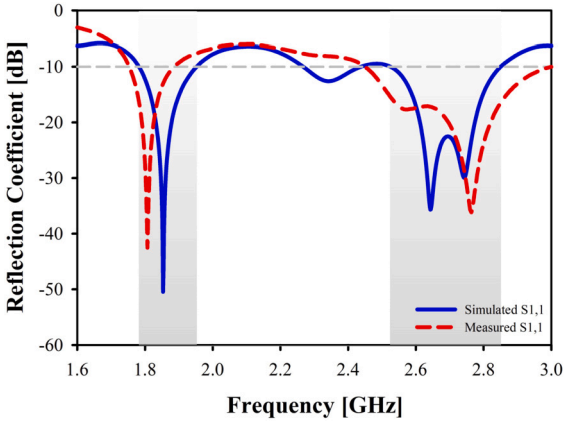

Fig. 9. Simulated and Measured Reflection coefficient of the proposed Antenna.

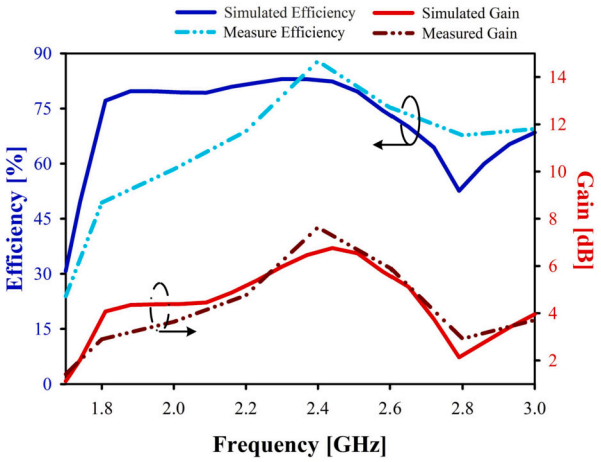

Fig. 10. Simulated and Measured Gain & Efficiency for the proposed antenna.

the SMA connector is utilized. It demonstrates that the simulated and measured resonance frequencies are not too far apart from one another.

When analyzing the performance of an antenna, two essential aspects that need to be taken into consideration are the antenna's gain as well as its directivity. The term "gain" refers to the amount of energy that is transmitted to the primary beam, while "directivity" refers to the amount of energy that is focused in a single direction [39]. The suggested Yagi antenna system's radiation efficiency and gain are measured and compared to their simulated counterpart. According to Fig. 10, the recommended antenna achieves a simulated maximum gain of 6.76 dB while also maintaining a maximum efficiency of 83.05%. Measurements of the prototype's peak gain in an anechoic chamber came in at 7.64 dB, with optimum efficiency of around 88%.

Fig. 11 illustrates the Z-matrix, which is still another essential element of the impedance characteristics of the proposed Yagi antenna. According to this figure, the real portion of the Z-parameter is close to 50 at 1.85 GHz and 2.64 GHz frequencies, while the imaginary part of the Z-parameter is close to 0 at both of those frequencies.

Fig. 12 shows the simulated and measured 2D radiation patterns at 1.85 and 2.64 GHz, respectively. At the first operating frequency, in the E-field, the main lobe magnitude at φ = 0 degree is 14.2 dBV/m, and the 3 dB angular beam width at φ = 90 degree is 151.4° at 1.8 GHz. In the case of H-field, the main lobe magnitude at φ = 0 degree is -37.3 dBA/m, and the 3 dB angular beam width at φ = 90 degree is 93° at 1.8 GHz.

At the second operating frequency, in the E-field, the prime lobe magnitude at φ = 0 degree is 14.4 dBV/m, and the 3 dB angular beam width at φ = 90 degree is 59.3° at 2.6 GHz. In the case of H-field, the

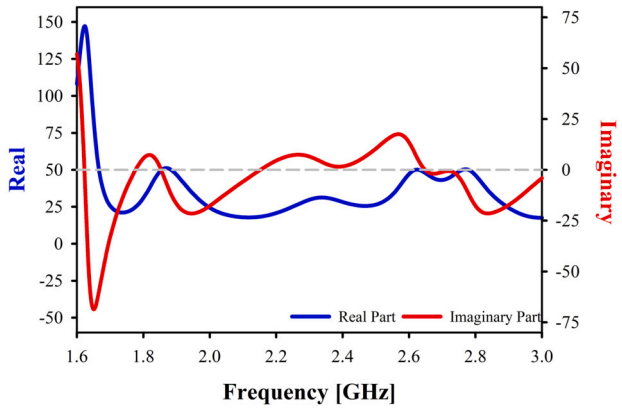

Fig. 11. Z-parameter of the studied antenna.

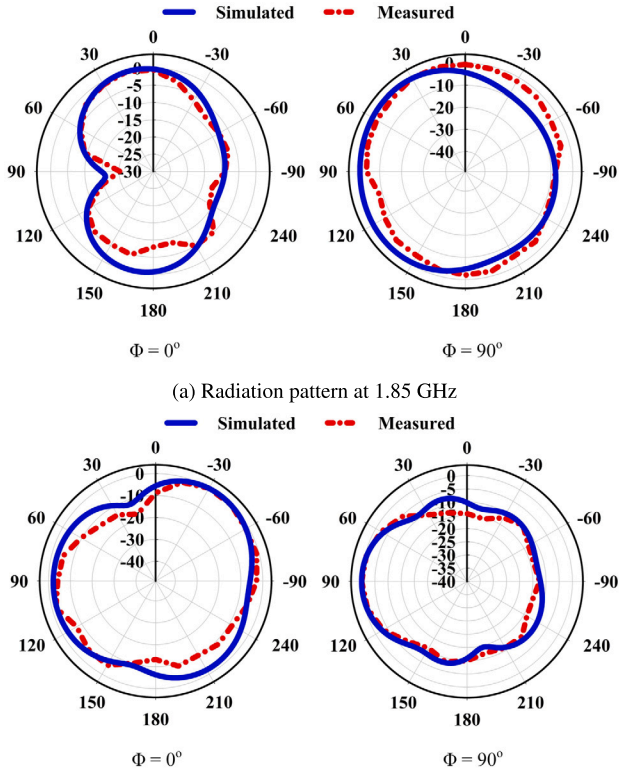

(a) Radiation pattern at 1.85 GHz

(b) Radiation pattern at 2.64 GHz

Fig. 12. Simulated and Measured Normalized Radiation patterns.

main lobe magnitude at φ = 0 degree is -37.1 dBA/m, and the 3 dB angular beam width at φ = 90 degree is 59.3° at 2.6 GHz.

The measured and simulated both E field (yz plane) and H field (xz plane) radiation patterns of the Yagi antenna are projected at angles between 0 and 90 degrees. However, due to measurement setup restrictions and faults in the 3D Yagi antenna, a minor disparity between simulated and measured findings is studied in both planes.

6.1. Equivalent circuit modeling and simulation

The equivalent circuit of the antenna is derived from the impedance analysis tools of the designed antenna using CST Studio simulation and circuit design tools in Agilent ADS software. Maximum power transfer (at least 90%) from the input port to the antenna structure and radiation into free space is guaranteed by a return level of less than -10 dB at the resonance frequency. When the impedance of the antenna circuit is matched to the characteristic impedance of 50 Ω, the maximum amount of power can be transferred. According to the principle of maximum power transmission, for a network to be considered "matched," the load impedance and the input resistance (Z_{load} = R_{in}) should be as close to equal as possible [40].

The approach relies on locating a lumped element model (RLC circuit) with close enough characteristics to the proposed Yagi antenna to be helpful. An equivalent circuit is suggested for each component of the designed antenna, as depicted in Fig. 13 (a), (b), (c), and the antenna is then reassembled as depicted in Fig. 13 (d) [41,42]. In the final step, a simulation is performed using the R L C parameters to cover the complete frequency range using the equivalent circuit model of the proposed antenna, as shown in Fig. 14. This model reproduces, to a close approximation, the behavior of the proposed Yagi antenna. Fig. 15 compares the analogous circuit simulation results with the CST simulation outcomes for the S11 parameters.

6.1.1. Equivalent circuits of feed line of Yagi antenna

The Yagi antenna under consideration was constructed using transmission lines, as depicted in Fig. 13 (a), as an integral component of its equivalent circuit. As a result, the feedline of the antenna replicates a circuit consisting of a parallel combination of R1, L1, and C1, with values of 48 Ω, 20 nH, and 2.4 pF, respectively.

6.1.2. Equivalent circuits of balun resonator and driving element

Fig. 13 (b) illustrates that the right side of the balun resonator is represented by the parallel components of R2 (30 Ω), L2 (11 nH), and C2 (1 pF), while the left side of the balun resonator is indicated by the shunt components of R3 (60 Ω), L3 (2 nH), and C3 (1 pF). The capacitance value of the internal gap separating the two balun resonators is C9 = 0.001 pF. As a result, the right dipole element of the antenna emulates a parallel circuit with values of R4 = 35 Ω, L4 = 7 nH, and C4 = 1 pF. Similarly, the left dipole element of the proposed antenna generates a parallel circuit with values of R5 = 35 Ω, L5 = 7 nH, and C5 = 1 pF. The capacitance values C11 = 4.2 pF and C12 = 4.2 pF indicate the separation between the dipole and director1, while C10 = 0.01 pF represents the internal gap between the dipoles, as illustrated in Fig. 13 (d).

6.1.3. Equivalent circuits of directors

As shown in Fig. 13 (c), the combination of C6 = 0.99 pF and L6 = 3 nH represents the first director, C7 = 0.97 pF and L7 = 3.5 nH represents the second director, and C8 = 0.95 pF and L8 = 4 nH represents the third director. All three of these combinations are used in conjunction with one another to represent the respective directors. As can be seen in Fig. 13 (d), the distance between directors 1 and 2 is represented by the symbol C13 = 0.9 pF, while the gap between directors 2 and 3 is represented by the letter C14 = 0.9 pF.

6.2. Machine learning methodology

Since ML techniques may be trained with either real-world or simulated antenna data, they have been the subject of extensive study and implementation in antenna design during the past decade. ML-assisted optimization (MLAO) involves constructing a computationally efficient model with ML approaches to predict the designated features at the potential places in the design space by using the training set obtained at the sampled points based on the initial computationally expensive model. Some examples of ML techniques used in MLAO strategies for antenna design are Gaussian process regression (GPR), support vector machine (SVM), and artificial neural networks analyzed in [43]. To present a high-level perspective, we might say that machine learning is the process of gaining insight from data by creating reliable prediction algorithms. These methods may be effective in optimization settings, but their performance will depend on the depth and breadth of the

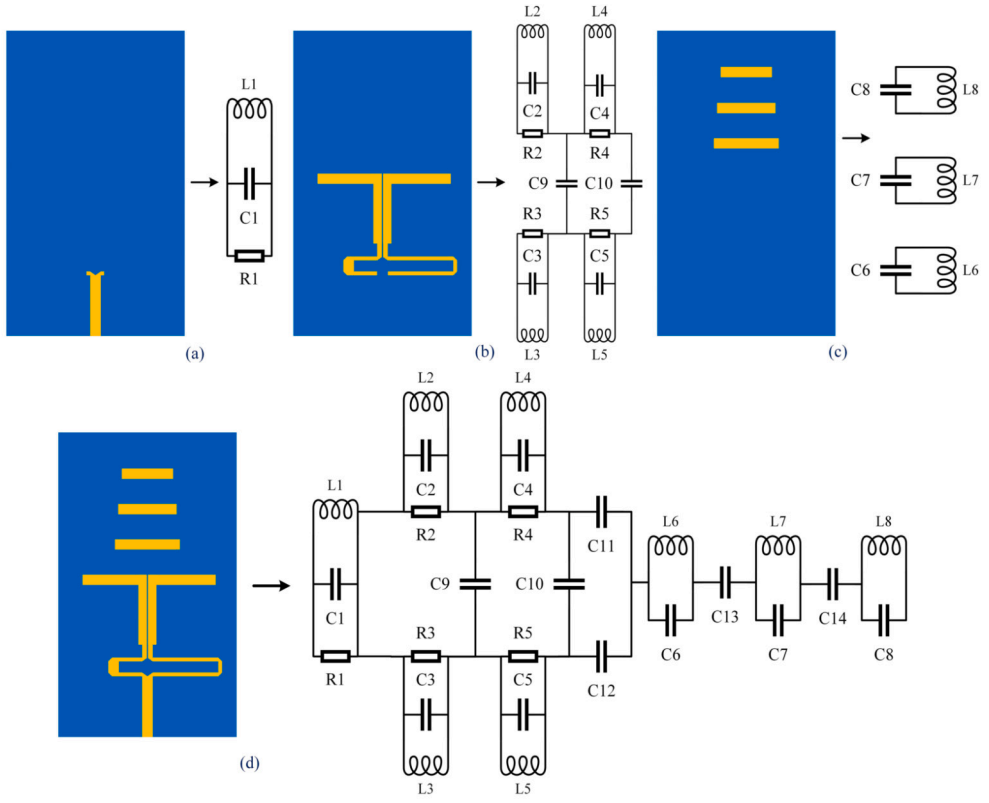

Fig. 13. Evolution of equivalent circuit of Yagi antenna: (a) Circuit model for feedline (b) Circuit model for box resonator (c) Circuit model for three directors (d) Final obtained equivalent circuit model.

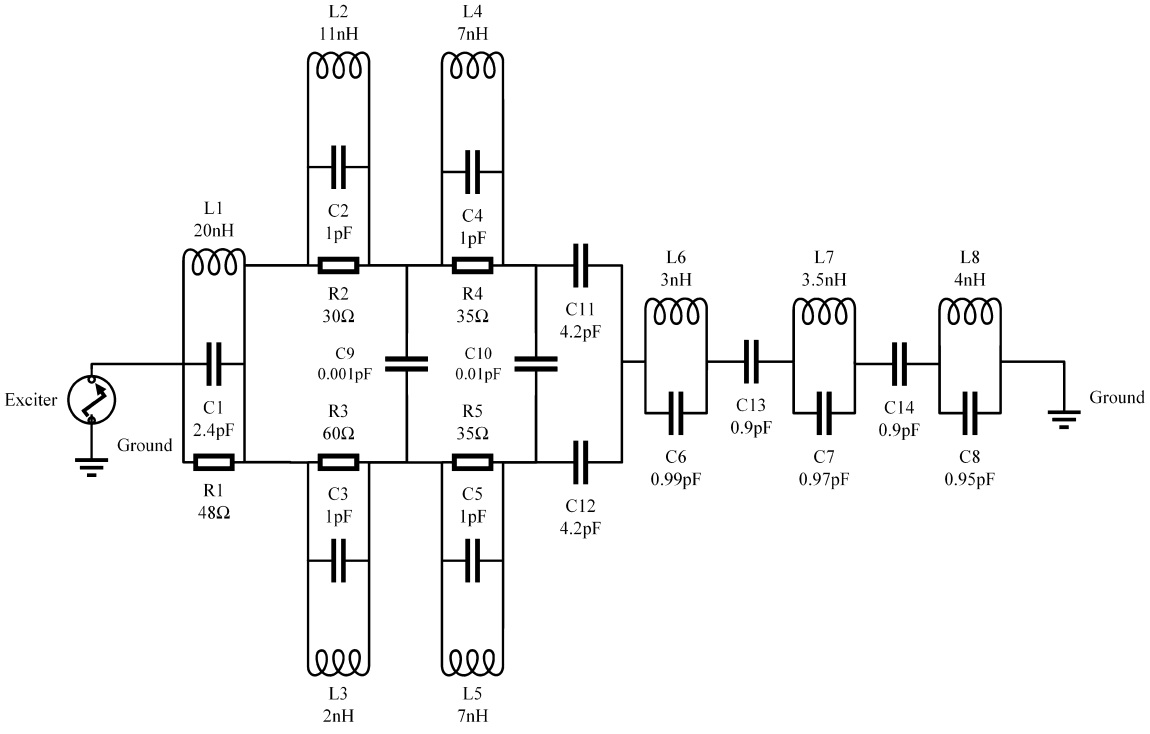

Fig. 14. Final equivalent circuit model after adjusting resistance, capacitance, and inductance values.

information available to them. This is why many people mistakenly believe that machine learning and statistical analysis are the same thing [44]. Since regression methods' ML assessment is significantly faster than the numerical solution of a physical simulation model, they are helpful for speeding up the optimization process. Regression models are also useful for pinpointing which specific design decisions led to the desired outcomes [45].

There are two parts to the methodology. The first phase involves using CST, a piece of simulation software, to construct an antenna that operates in the LTE frequency band and to extract the dataset generated

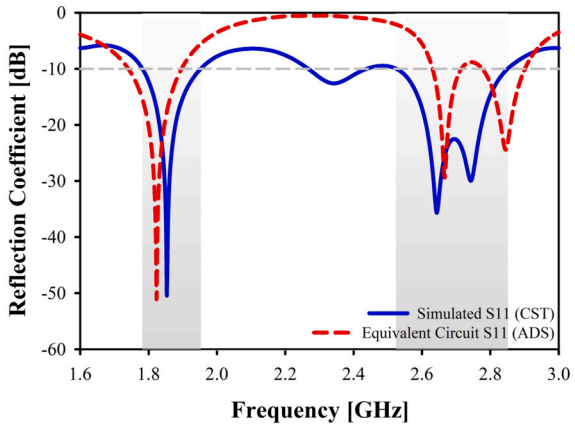

Fig. 15. Simulated reflection coefficient of the equivalent circuit in ADS and CST.

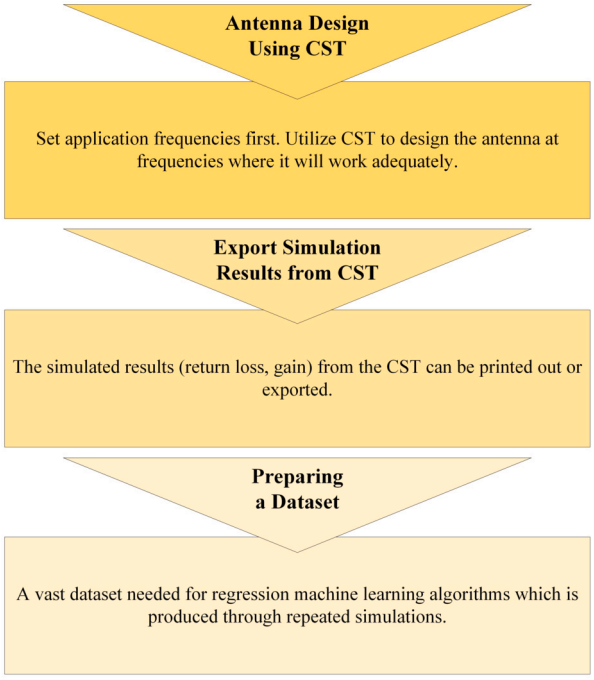

Fig. 16. Data acquisition workflow for Machine Learning.

by a parametric sweep. To determine which machine learning model will yield the best results, it must first be trained on the dataset.

Fig. 16 depicts the methods that will now be explored in further depth. First, choose an LTE frequency range between 1.85 and 2.64 GHz. At frequencies where the antenna's capability is adequate, use CST to design the antenna. Parametric sweeps allow for the export of simulated CST characteristics such as director length, dipole size, ground and reflector length, and so on. Regression machine learning methods may benefit from larger datasets in some circumstances, but this is not always the case. The extent to which a larger dataset influences a regression model depends on a number of parameters, including the difficulty of the problem, the dimensionality of the input characteristics, and the complexity of the model. Finally, 90 data samples are gathered via the simulation with the help of CST MWS, and a number of regression machine learning (ML) techniques are used to make predictions about the gain and resonant frequency of the proposed Yagi antenna. Using the train-test split strategy, the dataset can be segmented for use in both development and verification. This strategy uses a statistically-sound random partitioning of the data set into training and testing subsets.

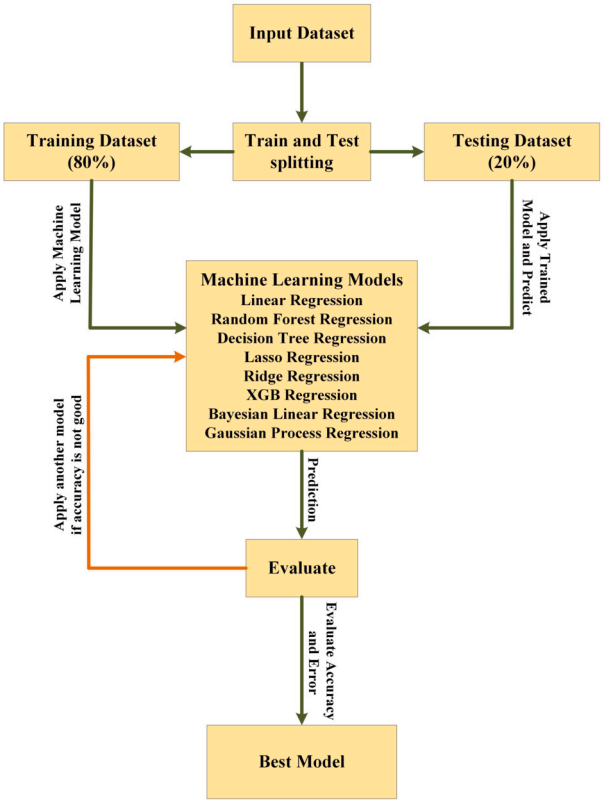

Fig. 17. Schematic depicting the steps required to develop a machine learning algorithm.

Eight different machine-learning algorithms are used to make predictions in this study. Linear Regression, Random Forest Regression, Decision Tree Regression, Lasso Regression, Ridge Regression, XGB Regression, Bayesian Linear Regression, and Gaussian Process Regression are only a few of the regression models being considered. These algorithms are chosen because of their proficiency in non-linear regression analysis. Since the end goal of implementing predictions is numbering, regression is the best method to use. The term "error" refers to the most commonly used statistic in regression analysis. Fig. 17 illustrates the steps in creating a machine learning algorithm as a flowchart. Parametric sweeps run on the CST simulation software were used to divide the dataset into two separate subsets for analysis. All of the machine learning research was carried out in Google Colab, Google's Python simulation. Using the sci-kit learn machine learning framework, we were able to build the Regression models quickly. Every study and visualization, but especially the conclusion, made use of Matplotlib.

The first portion of the study followed the recommendation in [46] and set aside 80% of the dataset for training, whereas the second half set aside 20% of the dataset for testing. Then, a machine-learning algorithm that takes into account the features and labels is applied to the training dataset. Once model training and cross-validation are complete, the model may be used to reliably predict inputs such as realized gain and directivity. Machine learning (ML) allows for more rapid and precise forecasting than may be achieved with computer simulation technology (CST). Gain prediction is best served by Ridge Regression model, while directivity is best served by Gaussian Process Regression.

6.3. *Machine learning model selection*

Using many different models can help assure the highest level of performance possible. Regression analysis [47] is a statistical method for assessing the relationship between variables with a cause-and-effect relationship. Although our problem is addressed through regression

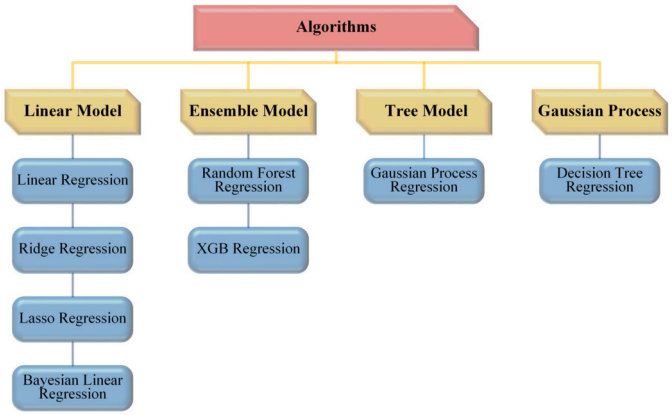

Fig. 18. Splitting of Regression Algorithms.

analysis, So, we used the eight most practical machine learning regression models, such as linear, tree, ensemble, and Gaussian process-based methods shown in Fig. 18. Each of these is described briefly below.

6.3.1. Linear regression

Linear regression [48] aims to model the relationship between two variables by fitting a linear equation to observable data. The first variable is an explanatory variable, whereas the second is the dependent variable.

6.3.2. Random forest regression

An ensemble system called Random Forest [49] can address both classification and regression issues. It achieves this by combining a technique known as Bootstrap and Aggregation, often known as bagging, with several decision trees.

6.3.3. Decision tree regression

Decision tree develops regression or classification methods using a tree structure. In decision tree regression [50], the properties of an item are analyzed, and a model is trained to fit inside the structure of a tree. This model is then used to predict data that will occur in the future and continuously produce meaningful output.

6.3.4. Lasso regression

As an approach to regression analysis in the disciplines of machine learning algorithms, lasso [51] (an acronym for least absolute shrinkage and selection operator) is commonly used. Combining variable selection with regularization, this strategy enhances the resultant statistical model's predictive power and human explainability.

6.3.5. Ridge regression

A method known as Ridge Regression [52] is used to analyze the results of multiple regressions when those results contain multicollinearity. In this manner, the L2 regularization procedure is executed. The projected quantities and actual numbers might diverge significantly when multicollinearity problems occur, least-squares approaches provide unbiased findings, and variances are significant.

6.3.6. XGB regression

XGBoost [53] is a powerful realization of the gradient-boosting algorithm with several useful applications, one of which is predictive regression modeling. An efficient application of XGBoost is in the creation of supervised regression analysis.

6.3.7. Bayesian linear regression

Bayesian linear regression [54] is a type of conditional modeling in which the mean of one variable is described by a linear combination of other variables. The prior probability of the regression analysis, dependent on the observed data of the regressors, is the goal of this modeling approach. It will also enable the out-of-sample forecast of the regression.

6.3.8. Gaussian process regression

Nonparametric kernel-based probabilistic models are known as Gaussian process regression (GPR) [55] models. It is a general-purpose supervised learning method with the purpose of resolving issues involving regression and probabilistic classification.

6.4. Performance measurement metrics

Error is the most commonly used metric in regression. We compared all the algorithms using numerous statistical metrics for measuring, evaluating, and analyzing their performance. We will go through each of them in depth in the following paragraphs.

The mean absolute error (MAE) figures out the average difference between the calculated and the found values. Equation (2) depicts the MAE [56] formulation.

$$MAE = \frac{1}{n}\sum_{i=1}^{n}\left|y_i - \hat{y}_i\right| \tag{2}$$

Where n is the total number of observations, $\hat{y}_i$ and y_i represent the predicted and actual values.

The most common form of the regression loss function is the mean squared error (MSE). The loss is calculated as the average over all data points of the squared disparities between the actual and forecasted values. The MSE [57] formulation is shown in Equation (3).

$$MSE = \frac{1}{n}\sum_{i=1}^{n}\left(y_i - \hat{y}_i\right)^2 \tag{3}$$

The mean squared logarithmic error (MSLE) can be regarded as a ratio of the true and predicted values. The MSLE [58] equation is shown in Equation (4).

$$MSLE = \frac{1}{n}\sum_{i=1}^{n}\left(\log\left(y_a\right) - \log\left(y_p\right)\right)^2 \tag{4}$$

Root Mean Squared Logarithmic Error (RMSLE) restores the unit to its original value by taking the Root of MSLE. The equation of RMSLE [59] is shown in Equation (5).

$$\text{RMSLE} = \sqrt{\left(\log\left(y_i + 1\right) - \log\left(\hat{y}_i + 1\right)\right)^2} \tag{5}$$

The mean absolute percentage error (MAPE) can be computed by first determining the difference between the actual value and the predicted value and then dividing it by the actual value. Equation (6) depicts the MAPE [60] formula.

$$\text{MAPE} = \frac{100\%}{n}\sum_{i=1}^{n}\left|\frac{y_i - \hat{y}_i}{y_i}\right| \tag{6}$$

The R-squared value indicates the accuracy of the model fit. When R^2 is close to 1, it indicates that the model provides a good fit for the data, whereas when it is closer to 0, it is a sign that the model is not very accurate. When a model predicts an absurd outcome, R-squared can be negative. R-squared [61] is expressed in equation (7).

$$R^2 = 1 - \frac{\sum_{i=1}^{N}\left(y_i - \hat{y}_i\right)^2}{\sum_{i=1}^{N}\left(y_i - \hat{y}_i\right)^2} \tag{7}$$

The explained variance score [62] describes the error dispersion in each dataset. It is defined as in equation (8).

$$\text{explained varience}\ (y, \hat{y}) = 1 - \frac{\text{Var}(y - \hat{y})}{\text{Var}(y)} \tag{8}$$

Table 2
Gain prediction performance.

Algorithms	MAE	MSE	MSLE	RMSLE	MAPE	R-Square	VarScore
Linear Regression	4.8250%	1.0547%	0.0957%	3.0934%	1.8435%	97.7871%	97.7897%
Random Forest Regression	9.4133%	1.7247%	0.1231%	3.5080%	3.3104%	96.3814%	96.3909%
Decision Tree Regression	11.1350%	3.0525%	0.2788%	5.2801%	4.1149%	93.5958%	93.7402%
Lasso Regression	13.7971%	2.8673%	0.1845%	4.2958%	4.5357%	93.9843%	94.0102%
Ridge Regression	4.7062%	1.0002%	0.0904%	3.0066%	1.7944%	97.9015%	97.9078%
XGB Regression	10.1547%	2.0270%	0.1806%	4.2496%	3.6217%	95.7472%	95.7781%
Bayesian Linear Regression	4.7272%	1.0440%	0.0948%	3.0788%	1.8166%	97.8096%	97.8129%
Gaussian Process Regression	4.7842%	1.0471%	0.0950%	3.0821%	1.8302%	97.8031%	97.8058%

Table 3
Simulated and predicted gain comparison on the test set using Ridge Regression.

No.	Simulated Gain	Predicted Gain	Error Percentage	No.	Simulated Gain	Predicted Gain	Error Percentage
1	3.42909	3.45668	0.80%	10	3.77284	3.78143	0.23%
2	3.71054	3.75020	1.07%	11	3.18975	3.21559	0.81%
3	3.91600	3.92045	0.11%	12	3.96585	3.96424	0.04%
4	4.57052	4.54707	0.51%	13	3.43816	3.43816	0%
5	3.78020	3.75045	0.79%	14	2.43987	2.51473	0.307%
6	2.32203	2.40160	3.43%	15	2.07540	2.17423	0.476%
7	3.75053	3.74762	0.08%	16	4.09692	4.09908	0.05%
8	3.69627	3.69188	0.12%	17	2.50593	2.11448	1.562%
9	4.37569	4.35639	0.44%	18	3.47866	3.49136	0.36%

Table 4
The Directivity prediction performance.

Algorithms	MAE	MSE	MSLE	RMSLE	MAPE	R-Square	VarScore
Linear Regression	5.0002%	1.4057%	0.0352%	1.8752%	0.9674%	96.8752%	96.8928%
Random Forest Regression	6.8659%	1.3553%	0.0378%	1.9447%	1.3387%	96.9872%	97.3368%
Decision Tree Regression	13.7062%	7.6193%	0.2073%	4.5531%	2.7260%	83.0630%	85.0300%
Lasso Regression	14.5382%	3.2877%	0.0779%	2.7915%	2.6144%	92.6918%	92.8456%
Ridge Regression	4.7999%	1.1393%	0.0282%	1.6801%	0.9008%	97.4674%	97.5155%
XGB Regression	10.4854%	2.8428%	0.0829%	2.8784%	2.0460%	93.6808%	93.9304%
Bayesian Linear Regression	4.8859%	1.3409%	0.0335%	1.8301%	0.9419%	97.0194%	97.0426%
Gaussian Process Regression	5.9301%	0.7943%	0.0190%	1.3770%	1.0612%	98.2343%	98.3110%

6.5. Gain prediction

Table 2 summarizes the relative merits of various regression methods, including linear, random forest, decision tree, lasso, ridge, XGB, Bayesian linear, and Gaussian process approaches. The accuracy performance of each algorithm is measured using the mean absolute error (MAE), mean squared error (MSE), mean root-mean-squared error (RMSLE), mean absolute percentage error (MAPE) R-squared, and variance score. Moreover, the performance comparison of these models is presented using a bar diagram in Fig. 19. It is shown that the RR model produces small errors for MAE, MSE, MSLE, RMSLE, and MAPE, with scores of 4.7062%, 1.0002%, 0.0904%, 3.0066%, and 1.7942%, respectively. In contrast, Ridge Regression has the best R-squared and variance score accuracy (97.9015% and 97.9078%, respectively). The simulated and predicted gains for 18 test samples using ridge regression (RR) are displayed in Fig. 20. In the study, we tune the frequency between 1.6 GHz and 3 GHz. Table 3 displays that the difference between the observed and expected gain for RR is negligible (very near to 0). Additionally, the error rate is typically less than 1%. Therefore, as can be seen in Fig. 20, the predicted outcome closely tracks the simulated result. Therefore, RR is chosen since it outperforms competing ML models in terms of gain prediction.

6.6. Directivity prediction

Table 4 summarizes the relative merits of various regression methods, including linear, random forest, decision tree, lasso, ridge, XGB, Bayesian linear, and Gaussian process approaches. The accuracy performance of each algorithm is measured using the mean absolute error (MAE), mean squared error (MSE), mean root-mean-squared error (RMSLE), mean absolute percentage error (MAPE) R-squared, and the variant score. It has been demonstrated that the GPR model generates relatively insignificant errors for MSE, MSLE, and RMSLE, with scores of 0.7943 percent, 0.019 percent, and 1.37 percent, respectively. When evaluating at MAE, bayesian linear regression gives the lowest error. However, when considering MAPE, linear regression displays the lowest error. However, the Gaussian Process Regression has the highest accuracy for both the R-squared and the variance score (98.23% and 98.11%, respectively). Moreover, the performance comparison of these models is presented using a bar diagram in Fig. 21. Each of the 18 test samples was run through the Gaussian Process Regression (GPR) method, and the simulated and predicted directivity is shown in Fig. 22. We customize the frequency to be somewhere between 1.6 and 3 gigahertz for the study. According to what is shown in Table 5, there is hardly any deviation between the actual and predicted levels of directivity for the GPR model (very near to 0). In addition to that, the percentage of errors is often lower than 1%. As a result, the simulated result and the predicted outcome are depicted in Fig. 22 in a very similar manner. Therefore, given its superior performance compared to other ML models in directivity prediction, GPR has been selected.

6.7. Statistical tests

In the Wilcoxon test, the p-value indicates the likelihood of observing the test statistic (the sum of ranks) or a more extreme number when the null hypothesis is accepted [63]. No significant difference exists between the two samples or observations, as stated by the null hypothesis. How likely it is that the test statistic (F-value) or a more extreme result

Table 5
Simulated and predicted directivity comparison on the test set using Gaussian Process Regression.

No.	Simulated Directivity	Predicted Directivity	Error Percentage	No.	Simulated Directivity	Predicted Directivity	Error Percentage
1	5.54311	5.60121	1.05%	10	6.23284	6.23176	0.02%
2	6.24775	6.12147	2.02%	11	5.60286	5.66676	1.14%
3	6.28841	6.24887	0.63%	12	6.29931	6.25179	0.75%
4	6.94375	6.98022	0.53%	13	5.54853	5.63823	1.62%
5	6.19702	6.21144	0.23%	14	4.87025	4.83760	0.67%
6	4.75591	4.84679	1.91%	15	4.49189	4.47738	0.32%
7	6.17642	6.17988	0.06%	16	6.37744	6.28637	1.43%
8	6.18115	6.21868	0.61%	17	5.15692	5.45115	5.71%
9	6.77792	6.79011	0.18%	18	5.91079	5.89689	0.24%

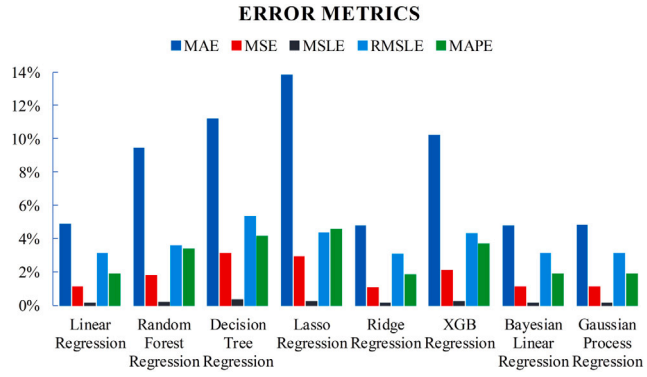

(a) Error Metrics comparative bar chart of ML regressors (Gain)

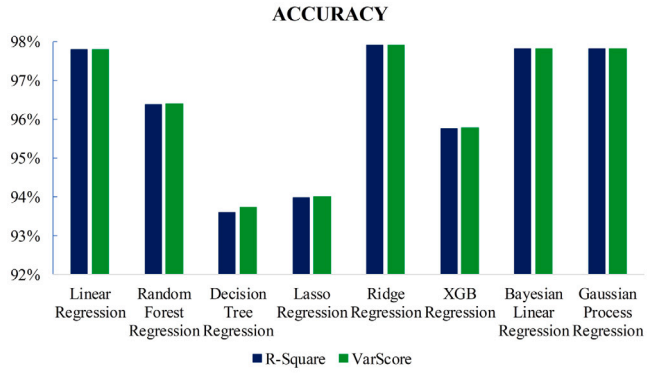

(b) Accuracy comparative bar chart of ML regressors (Gain)

Fig. 19. Performance comparative bar chart of ML regressors (Gain).

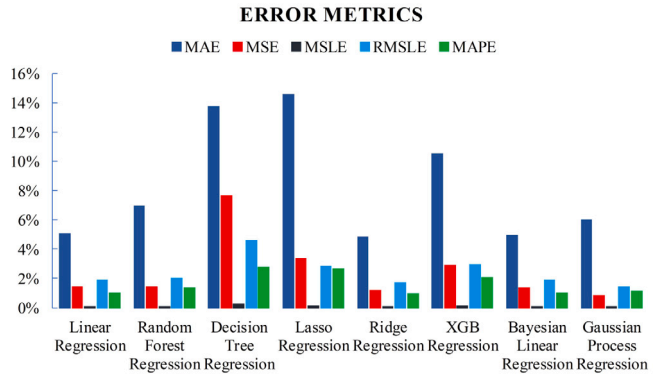

(a) Error Metrics comparative bar chart of ML regressors (Directivity)

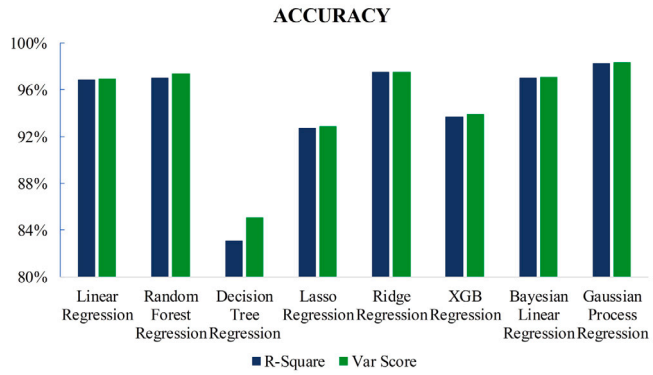

(b) Accuracy comparative bar chart of ML regressors (Directivity)

Fig. 21. Performance comparative bar chart of ML regressors (Directivity).

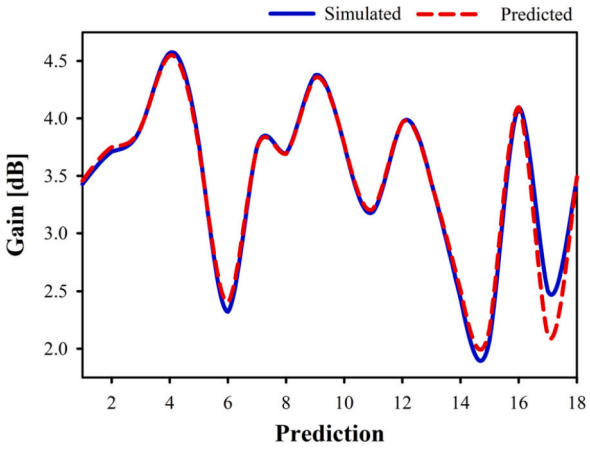

Fig. 20. Simulated vs predicted gain using Ridge Regression.

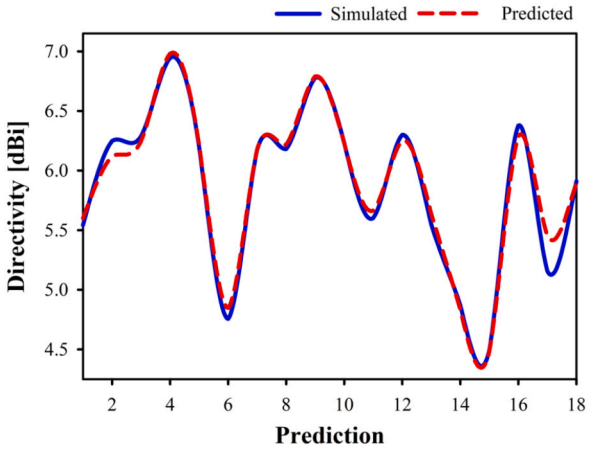

Fig. 22. Simulated vs predicted directivity using Gaussian Process Regression.

will be found in an analysis of variance (ANOVA) is indicated by the p-value. Under the null hypothesis of ANOVA, the means of the groups being compared will be found to be the same.

Whether or whether an observed difference is statistically significant is often assessed by comparing the p-value to a preset significance level (such as 0.05) [64]. Evidence against the null hypothesis, in the form of a p-value below the significance level, would show that the paired observations or samples are significantly different from one another. However, if the p-value is larger than the significance level, it indicates that there is not enough evidence to reject the null hypothesis and that there is no difference. Our p-values for the Wilcoxon test of the ridge regression are 0.303794, and the p-values for the analysis of variance test are 0.9817, so there is no significant difference between the two tests. We find no statistically significant difference between the Wilcoxon test's p-value of 0.5798 and the ANOVA test's p-value of 0.9348 for the Gaussian Process Regression.

6.8. Limitations of this work

To achieve a high gain level, a long Yagi antenna is required, but it also has a number of drawbacks. A high-gain Yagi antenna requires a combination of some directors and some other types of elements in order to work. Although the antenna in the suggested design is quite large ($130 \times 119.30 mm^2$), its gain and efficiency have been greatly improved. A larger number of director elements in an array reduces the available bandwidth. Although a long antenna might enhance reception, it also raises the possibility of interference. We have designed and analyzed an equivalent RLC circuit for the proposed Yagi antenna using the ADS simulation tool. The regression model is another contributing part of this work. For the simulation, 90 data samples are collected using CST MWS, and these data are then subjected to a number of regression machine learning (ML) approaches. Due to a lack of training data, we do not apply deep learning models like CNN or ANN.

7. Conclusion and future directions

To assess the performance for the expected LTE applications, this study effort incorporates a Quasi-Yagi antenna design, modeling, measurement of the produced antenna prototype, equivalent RLC circuit analysis, and various machine learning techniques. The proposed antenna was first designed using the CST simulation tool, and it has a maximum gain of 6.76 dB, a maximum directivity of 8.21 dBi, and a maximum efficiency of 83.05% for cellular communication in the LTE frequency spectrum at 1.85 GHz and 2.64 GHz. Additionally, the RLC equivalent circuit model of the antenna developed by ADS Agilent and the CST-simulated antenna design offers nearly identical performances. Furthermore, eight different regression models have also been applied to determine the gain and directivity of the antenna. The data samples are strikingly comparable when anticipated and simulated results are compared. To validate the prediction made by the supervised regression algorithms, multiple performance measures, including MAE, MSE, MSLE, RMSLE, and MAPE, as well as R square and variance scores, are computed. These metrics are referred to as "performance metrics". According to extensive analyses and acquired results, the ridge regression model outperforms other models' accuracy for gain prediction, whereas the gaussian process regression model performs best for directivity prediction. The results from simulation and measurement are quite compatible with one another, and the developed Quasi-Yagi antenna covers the desired LTE frequency spectrum. The simulation, measurement, and predicted results corroborate the proposed Quasi-Yagi antenna's suitability for LTE applications. By utilizing low-loss dielectric material, the antenna might eventually be further reduced in size without sacrificing a greater efficiency level. To ensure further performance improvement, multi-substrate techniques and an increase in the number of directors could be used.

Declaration of competing interest

The authors declare that they have no known competing financial interests or personal relationships that could have appeared to influence the work reported in this paper.

Acknowledgement

This study is supported via funding from Prince Sattam bin Abdulaziz University project number (PSAU/2023/R/1444)

References

[1] S.S. Al-Bawri, M.T. Islam, T. Shabbir, G. Muhammad, M.S. Islam, H.Y. Wong, Hexagonal shaped near zero index (NZI) metamaterial based MIMO antenna for millimeter-wave application, IEEE Access 8 (2020) 181003–181013, https://doi.org/10.1109/ACCESS.2020.3028377, https://ieeexplore.ieee.org/document/9211507/.

[2] R. Przesmycki, M. Bugaj, L. Nowosielski, Broadband microstrip antenna for 5G wireless systems operating at 28 GHz, Electronics 10 (1) (2020) 1, https://doi.org/10.3390/electronics10010001, https://www.mdpi.com/2079-9292/10/1/1.

[3] S. Padmanathan, A. Abdullah Al-Hadi, A.M. Elshirkasi, S.S. Al-Bawri, M.T. Islam, T. Sabapathy, M. Jusoh, P. Akkaraekthalin, P.J. Soh, Compact multiband reconfigurable MIMO antenna for sub- 6 GHz 5G mobile terminal, IEEE Access 10 (2022) 60241–60252, https://doi.org/10.1109/ACCESS.2022.3180048, https://ieeexplore.ieee.org/document/9787554/.

[4] I. Messaoudene, T.A. Denidni, A. Benghalia, CDR antenna with dual-band 1.9/2.7 GHz for MIMO-LTE terminals, Microw. Opt. Technol. Lett. 57 (10) (2015) 2388–2391, https://doi.org/10.1002/mop.29334, https://onlinelibrary.wiley.com/doi/10.1002/mop.29334.

[5] M. Elahi, Irfanullah, R. Khan, A. Abdullah Al-Hadi, S. Usman, P.J. Soh, A dual-band planar quasi Yagi-Uda antenna with optimized gain for LTE applications, Prog. Electromagn. Res. C 92 (2019) 239–250, https://doi.org/10.2528/PIERC19022401, http://www.jpier.org/PIERC/pier.php?paper=19022401.

[6] N. Kaneda, W. Deal, Yongxi Qian, R. Waterhouse, T. Itoh, A broadband planar quasi-Yagi antenna, IEEE Trans. Antennas Propag. 50 (8) (2002) 1158–1160, https://doi.org/10.1109/TAP.2002.801299, http://ieeexplore.ieee.org/document/1035006/.

[7] H.T. Chattha, M. Hanif, X. Yang, Q.H. Abbasi, I.E. Rana, Frequency reconfigurable patch antenna for 4G LTE applications, Prog. Electromagn. Res. M 69 (2018) 1–13, https://doi.org/10.2528/PIERM18022101, http://www.jpier.org/PIERM/pier.php?paper=18022101.

[8] W. Geyi, Foundations of Applied Electrodynamics, 1st edition, Wiley, 2010, https://onlinelibrary.wiley.com/doi/book/10.1002/9780470661369.

[9] G. Wen, Foundations for Radio Frequency Engineering, World Scientific, 2015, https://www.worldscientific.com/worldscibooks/10.1142/9040.

[10] A.D. Chaudhari, K. Ray, A single-layer compact four-element quasi-Yagi MIMO antenna design for super-wideband response, AEÜ, Int. J. Electron. Commun. 138 (2021) 153878, https://doi.org/10.1016/j.aeue.2021.153878, https://linkinghub.elsevier.com/retrieve/pii/S1434841121002752.

[11] Q. Xin, F.-S. Zhang, B.-H. Sun, Y.-L. Zou, Q.-Z. Liu, Yagi-Uda antenna with small size for vehicles, Electron. Lett. 47 (7) (2011) 428, https://doi.org/10.1049/el.2011.0148, https://digital-library.theiet.org/content/journals/10.1049/el.2011.0148.

[12] M.-C. Tang, T. Shi, R.W. Ziolkowski, Flexible efficient quasi-Yagi printed uniplanar antenna, IEEE Trans. Antennas Propag. 63 (12) (2015) 5343–5350, https://doi.org/10.1109/TAP.2015.2486807, http://ieeexplore.ieee.org/document/7289377/.

[13] R. Alhalabi, G. Rebeiz, High-gain Yagi-Uda antennas for millimeter-wave switched-beam systems, IEEE Trans. Antennas Propag. 57 (11) (2009) 3672–3676, https://doi.org/10.1109/TAP.2009.2026666, http://ieeexplore.ieee.org/document/5159519/.

[14] A.A. Abdulhameed, F.M. Alnahwi, H.N. Al-Anbagi, Z. Kubík, A.S. Abdullah, Frequency reconfigurable key-shape antenna for LTE applications, Aust. J. Electr. Electron. Eng. 20 (2) (2023) 138–146, https://doi.org/10.1080/1448837X.2022.2112316, https://www.tandfonline.com/doi/full/10.1080/1448837X.2022.2112316.

[15] M.A. Haque, M.A. Zakariya, N.S. Sawaran Singh, M.A. Rahman, L.C. Paul, Parametric study of a dual-band quasi-Yagi antenna for LTE application, Bull. Electr. Eng. Inform. 12 (3) (2023) 1513–1522, https://doi.org/10.11591/eei.v12i3.4639, https://beei.org/index.php/EEI/article/view/4639.

[16] M.Z. Mahmud, M. Samsuzzaman, L.C. Paul, M.R. Islam, A.A. Althuwayb, M.T. Islam, A dielectric resonator based line stripe miniaturized ultra-wideband antenna for fifth-generation applications, Int. J. Commun. Syst. 34 (5) (Mar. 2021), https://doi.org/10.1002/dac.4740, https://onlinelibrary.wiley.com/doi/10.1002/dac.4740.

[17] S. Kim, J. Choi, Quasi-Yagi slotted array antenna with fan-beam characteristics for 28 GHz 5G mobile terminals, Appl. Sci. 10 (21) (2020) 7686, https://doi.org/10.3390/app10217686, https://www.mdpi.com/2076-3417/10/21/7686.

[18] M.R. Soheilifar, Compact Yagi-Uda slot antenna with metamaterial element for wide bandwidth wireless application, Int. J. RF Microw. Comput.-Aided Eng. 31 (3) (Mar. 2021), https://doi.org/10.1002/mmce.22380, https://onlinelibrary.wiley.com/doi/10.1002/mmce.22380.

[19] K.M. Morshed, D.K. Karmokar, K.P. Esselle, Antennas for licensed shared access in 5G communications with LTE mid- and high-band coverage, Sensors 23 (4) (2023) 2095, https://doi.org/10.3390/s23042095, https://www.mdpi.com/1424-8220/23/4/2095.

[20] S.S. Shirabadagi, V.G. Kasabegoudar, A planar suspended multiband Yagi antenna for WLAN, LTE, and 5G wireless applications, Prog. Electromagn. Res. C 122 (2022) 141–151, https://doi.org/10.2528/PIERC22062303, http://www.jpier.org/PIERC/pier.php?paper=22062303.

[21] G.R. Friedrichs, D.S. Filipovi¢, M.A. Elmansouri, W.A. Shiroma, T.W. Barton, Y. Liu, Machine learning enhanced antenna systems, Tech. Rep.

[22] J.-S. Kim, D.-Y. Lee, T.-H. Kim, D.-W. Seo, Chaff cloud modeling and electromagnetic scattering properties estimation, IEEE Access 11 (2023) 58835–58849, https://doi.org/10.1109/ACCESS.2023.3284833, https://ieeexplore.ieee.org/document/10147780/.

[23] P. Ranjan, S. Yadav, H. Gupta, A. Bage, Design and development of machine learning assisted cylindrical dielectric resonator antenna, Evergreen 10 (1) (2023) 308–316, https://doi.org/10.5109/6781085, http://hdl.handle.net/2324/6781085.

[24] S. Sairam, D.S. Kumar, S. Sabapathi, S. Angali, Optimization of double ring frequency selective surface for sub 5G/X-band communications using supervised ML and DL algorithms, IEEE Trans. Electromagn. Compat. (2023) 1–6, https://doi.org/10.1109/TEMC.2023.3287581, https://ieeexplore.ieee.org/document/10164807/.

[25] A.H. Shah, K. Ghosh, P.N. Patel, Modeling and Optimization of CPW-Fed E-Textile Antenna Using Machine Learning Algorithms, Tech. Rep., vol. 130, 2023.

[26] J. Undrakonda, R.K. Upadhyayula, Effects of metamaterials on MIMO antennas for X-band radar applications and parameter optimization with a machine learning model: a review, AIP Adv. 13 (4) (2023) 040701, https://doi.org/10.1063/5.0142886, https://pubs.aip.org/adv/article/13/4/040701/2884960/Effects-of-metamaterials-on-MIMO-antennas-for-X.

[27] J. Tan, J. Zhang, E. Ball, Machine learning-assisted method for efficient and accurate antenna modelling, Tech. Rep.

[28] A. Aoad, Design and manufacture of a multiband rectangular spiral-shaped microstrip antenna using EM-driven and machine learning, Elektron. Elektrotech. 27 (1) (2021) 29–40, https://doi.org/10.5755/j02.eie.27583, https://eejournal.ktu.lt/index.php/elt/article/view/27583.

[29] Department of Electrical Engineering, Universitas Trisakti, DKI Jakarta 11440, Indonesia, N. Kurniawati, A. Fahmi, S. Alam, Predicting rectangular patch microstrip antenna dimension using machine learning, J. Commun. (2021) 394–399, https://doi.org/10.12720/jcm.16.9.394-399, http://www.jocm.us/show-259-1686-1.html, 2021.

[30] V.S. Kushwah, G.S. Tomar, Design and analysis of microstrip patch antennas using artificial neural network, in: S. Chattopadhyay (Ed.), Trends in Research on Microstrip Antennas, InTech, 2017, http://www.intechopen.com/books/trends-in-research-on-microstrip-antennas/design-and-analysis-of-microstrip-patch-antennas-using-artificial-neural-network.

[31] H.A. Shoeab, M.A. Mohamed, M. El Said A, A.A. Kabeel, Microstrip antenna design using CST optimized by neural network algorithm, Mansoura Eng. J. 48 (3) (Jan. 2023), https://doi.org/10.58491/2735-4202.3045, https://mej.researchcommons.org/home/vol48/iss3/4.

[32] E.S. Saçın, A.C. Durgun, Neural network modeling of antennas on package for 5G applications, in: 2023 17th European Conference on Antennas and Propagation (EuCAP), IEEE, Florence, Italy, 2023, pp. 1–5, https://ieeexplore.ieee.org/document/10133407/.

[33] Z. Awang, Microwave Systems Design, Springer Singapore, Singapore, 2014, http://link.springer.com/10.1007/978-981-4451-24-6.

[34] H. Karbalaee, M.R. Salehifar, S. Soleimany, Designing Yagi-Uda antenna fed by microstrip line and simulated by HFSS, in: 2012 6th International Conference on Application of Information and Communication Technologies (AICT), IEEE, Tbilisi, Georgia, 2012, pp. 1–5, http://ieeexplore.ieee.org/document/6398503/.

[35] J. Shi, L. Zhu, N.-W. Liu, W. Wu, A microstrip Yagi antenna with an enlarged beam tilt angle via a slot-loaded patch reflector and pin-loaded patch directors, Antennas Wirel. Propag. Lett. 18 (4) (2019) 679–683, https://doi.org/10.1109/LAWP.2019.2901033, https://ieeexplore.ieee.org/document/8649659/.

[36] A. Ramos, T. Varum, J. Matos, Compact multilayer Yagi-Uda based antenna for IoT/5G sensors, Sensors 18 (9) (2018) 2914, https://doi.org/10.3390/s18092914, http://www.mdpi.com/1424-8220/18/9/2914.

[37] D.S. Woo, Y.-K. Cho, K.W. Kim, Balance analysis of microstrip-to-CPS baluns and its effects on broadband antenna performance, Int. J. Antennas Propag. 2013 (2013) 1–9, https://doi.org/10.1155/2013/651040, http://www.hindawi.com/journals/ijap/2013/651040/.

[38] M.A. Haque, M.A. Zakariya, L.C. Paul, D. Nath, P. Biswas, R. Azim, Analysis of slotted E-shaped microstrip patch antenna for Ku band applications, in: 2021 IEEE 15th Malaysia International Conference on Communication (MICC), IEEE, Malaysia, 2021, pp. 98–101, https://ieeexplore.ieee.org/document/9642100/.

[39] M.A. Haque, L.C. Paul, S. Kumar, R. Azim, M.S. Hosain, M. Azman Zakariya, A plowing T-shaped patch antenna for WiFi and C band applications, in: 2021 International Conference on Automation, Control and Mechatronics for Industry 4.0 (ACMI), IEEE, Rajshahi, Bangladesh, 2021, pp. 1–4, https://ieeexplore.ieee.org/document/9528266/.

[40] D.M. Pozar, Microwave Engineering, John Wiley & Sons, 2011.

[41] S. Hannan, M.T. Islam, M.R.I. Faruque, M.E.H. Chowdhury, F. Musharavati, Angle-insensitive co-polarized metamaterial absorber based on equivalent circuit analysis for dual band WiFi applications, Sci. Rep. 11 (1) (2021) 13791, https://doi.org/10.1038/s41598-021-93322-5, https://www.nature.com/articles/s41598-021-93322-5.

[42] A. Hossain, M.T. Islam, N. Misran, M.S. Islam, M. Samsuzzaman, A mutual coupled spider net-shaped triple split ring resonator based epsilon-negative metamaterials with high effective medium ratio for quad-band microwave applications, Results Phys. 22 (2021) 103902, https://doi.org/10.1016/j.rinp.2021.103902, https://linkinghub.elsevier.com/retrieve/pii/S2211379721000814.

[43] P. Ranjan, H. Gupta, S. Yadav, A. Sharma, Machine learning assisted optimization and its application to hybrid dielectric resonator antenna design, Facta Univ., Electron. Energ. 36 (1) (2023) 31–42, https://doi.org/10.2298/FUEE2301031R, https://doiserbia.nb.rs/Article.aspx?ID=0353-36702301031R.

[44] X. Pan, X. Lin, D. Cao, X. Zeng, P.S. Yu, L. He, R. Nussinov, F. Cheng, Deep learning for drug repurposing: methods, databases, and applications, WIREs Comput. Mol. Sci. 12 (4) (Jul. 2022), https://doi.org/10.1002/wcms.1597, https://onlinelibrary.wiley.com/doi/10.1002/wcms.1597.

[45] M.A.H. Talpur, S.H. Khahro, T.H. Ali, H.B. Waseem, M. Napiah, Computing travel impendences using trip generation regression model: a phenomenon of travel decision-making process of rural households, Environ. Dev. Sustain. 25 (7) (2023) 5973–5996, https://doi.org/10.1007/s10668-022-02288-5, https://link.springer.com/10.1007/s10668-022-02288-5.

[46] Q.H. Nguyen, H.-B. Ly, L.S. Ho, N. Al-Ansari, H.V. Le, V.Q. Tran, I. Prakash, B.T. Pham, Influence of data splitting on performance of machine learning models in prediction of shear strength of soil, Math. Probl. Eng. 2021 (2021) 1–15, https://doi.org/10.1155/2021/4832864, https://www.hindawi.com/journals/mpe/2021/4832864/.

[47] M.A. Haque, N. Sarker, N.S. Sawaran Singh, M.A. Rahman, M.N. Hasan, M. Islam, M.A. Zakariya, L.C. Paul, A.H. Sharker, G.E.M. Abro, M. Hannan, R. Pk, Dual band antenna design and prediction of resonance frequency using machine learning approaches, Appl. Sci. 12 (20) (2022) 10505, https://doi.org/10.3390/app122010505, https://www.mdpi.com/2076-3417/12/20/10505.

[48] J. Chen, K. de Hoogh, J. Gulliver, B. Hoffmann, O. Hertel, M. Ketzel, M. Bauwelinck, A. van Donkelaar, U.A. Hvidtfeldt, K. Katsouyanni, N.A. Janssen, R.V. Martin, E. Samoli, P.E. Schwartz, M. Stafoggia, T. Bellander, M. Strak, K. Wolf, D. Vienneau, R. Vermeulen, B. Brunekreef, G. Hoek, A comparison of linear regression, regularization, and machine learning algorithms to develop Europe-wide spatial models of fine particles and nitrogen dioxide, Environ. Int. 130 (2019) 104934, https://doi.org/10.1016/j.envint.2019.104934, https://linkinghub.elsevier.com/retrieve/pii/S0160412019304404.

[49] D. Borup, B.J. Christensen, N.S. Mühlbach, M.S. Nielsen, Targeting predictors in random forest regression, Int. J. Forecast. (2022) S0169207022000395, https://doi.org/10.1016/j.ijforecast.2022.02.010, https://linkinghub.elsevier.com/retrieve/pii/S0169207022000395.

[50] M. Rakhra, P. Soniya, D. Tanwar, P. Singh, D. Bordoloi, P. Agarwal, S. Takkar, K. Jairath, N. Verma, WITHDRAWN: crop price prediction using random forest and decision tree regression:-a review, in: Materials Today: Proceedings, 2021, S2214785321022902, https://linkinghub.elsevier.com/retrieve/pii/S2214785321022902.

[51] M.B. van Egmond, G. Spini, O. van der Galien, A. IJpma, T. Veugen, W. Kraaij, A. Sangers, T. Rooijakkers, P. Langenkamp, B. Kamphorst, N. van de L'Isle, M. Kooij-Janic, Privacy-preserving dataset combination and Lasso regression for healthcare predictions, BMC Med. Inform. Decis. Mak. 21 (1) (2021) 266, https://doi.org/10.1186/s12911-021-01582-y, https://bmcmedinformdecismak.biomedcentral.com/articles/10.1186/s12911-021-01582-y.

[52] X. Wang, X. Wang, B. Ma, Q. Li, Y.-Q. Shi, High precision error prediction algorithm based on ridge regression predictor for reversible data hiding, IEEE Signal Process. Lett. 28 (2021) 1125–1129, https://doi.org/10.1109/LSP.2021.3080181, https://ieeexplore.ieee.org/document/9431657/.

[53] A. Ibrahem Ahmed Osman, A. Najah Ahmed, M.F. Chow, Y. Feng Huang, A. El-Shafie, Extreme gradient boosting (Xgboost) model to predict the groundwater levels in Selangor Malaysia, Ain Shams Eng. J. 12 (2) (2021) 1545–1556, https://doi.org/10.1016/j.asej.2020.11.011, https://linkinghub.elsevier.com/retrieve/pii/S2090447921000125.

[54] S.A. Baldwin, M.J. Larson, An introduction to using Bayesian linear regression with clinical data, Behav. Res. Ther. 98 (2017) 58–75, https://doi.org/10.1016/j.brat.2016.12.016, https://linkinghub.elsevier.com/retrieve/pii/S0005796716302364.

[55] E. Schulz, M. Speekenbrink, A. Krause, A tutorial on Gaussian process regression: modelling, exploring, and exploiting functions, J. Math. Psychol. 85 (2018) 1–16, https://doi.org/10.1016/j.jmp.2018.03.001, https://linkinghub.elsevier.com/retrieve/pii/S0022249617302158.

[56] H.K.S. Doreswamy, Y. Km, I. Gad, Forecasting air pollution particulate matter (PM2.5) using machine learning regression models, Proc. Comput. Sci. 171 (2020) 2057–2066, https://doi.org/10.1016/j.procs.2020.04.221, https://linkinghub.elsevier.com/retrieve/pii/S1877050920312060.

[57] S.A. Shetty, T. Padmashree, B.M. Sagar, N.K. Cauvery, Performance analysis on machine learning algorithms with deep learning model for crop yield prediction, in: I. Jeena Jacob, S. Kolandapalayam Shanmugam, S. Piramuthu, P. Falkowski-Gilski (Eds.), Data Intelligence and Cognitive Informatics, in: Algorithms for Intelligent

Systems, Springer Singapore, Singapore, 2021, pp. 739–750, http://link.springer.com/10.1007/978-981-15-8530-2_58.

[58] O. Istaiteh, T. Owais, N. Al-Madi, S. Abu-Soud, Machine learning approaches for COVID-19 forecasting, in: 2020 International Conference on Intelligent Data Science Technologies and Applications (IDSTA), IEEE, Valencia, Spain, 2020, pp. 50–57, https://ieeexplore.ieee.org/document/9264101/.

[59] L. Barua, M. Sharif, T. Akter, Analyzing cervical cancer by using an ensemble learning approach based on meta classifier, Int. J. Comput. Appl. Technol. 182 (46) (2019) 29–33, https://doi.org/10.5120/ijca2019918619, http://www.ijcaonline.org/archives/volume182/number46/barua-2019-ijca-918619.pdf.

[60] A. de Myttenaere, B. Golden, B. Le Grand, F. Rossi, Mean absolute percentage error for regression models, Neurocomputing 192 (2016) 38–48, https://doi.org/10.1016/j.neucom.2015.12.114, https://linkinghub.elsevier.com/retrieve/pii/S0925231216003325.

[61] A. Gelman, B. Goodrich, J. Gabry, A. Vehtari, R-squared for Bayesian regression models, Am. Stat. 73 (3) (2019) 307–309, https://doi.org/10.1080/00031305.2018.1549100, https://www.tandfonline.com/doi/full/10.1080/00031305.2018.1549100.

[62] J.M. Weiming, Mastering Python for Finance, Packt Publishing Ltd, 2015.

[63] D. Sami Khafaga, E.-S.M. El-kenawy, F. Khalid Karim, S. Alshetewi, A. Ibrahim, A.A. Abdelhamid, Optimized weighted ensemble using dipper throated optimization algorithm in metamaterial antenna, Comput. Mater. Continua 73 (3) (2022) 5771–5788, https://doi.org/10.32604/cmc.2022.032229, https://www.techscience.com/cmc/v73n3/49121.

[64] D.S. Khafaga, A.A. Alhussan, E.-S.M. El-Kenawy, A. Ibrahim, M.M. Eid, A.A. Abdelhamid, Solving optimization problems of metamaterial and double T-shape antennas using advanced meta-heuristics algorithms, IEEE Access 10 (2022) 74449–74471, https://doi.org/10.1109/ACCESS.2022.3190508, https://ieeexplore.ieee.org/document/9828401/.